GEOPHYSICS, VOL. 80, NO. 6 (NOVEMBER-DECEMBER 2015); P. B193–B202, 8 FIGS.
10.1190/GEO2014-0527.1

Case History

Boat-towed radio-magnetotellurics — A new technique and case study from the city of Stockholm

Mehrdad Bastani[1], Lena Persson[1], Suman Mehta[2], and Alireza Malehmir[2]

ABSTRACT

We have developed a new data acquisition system and technique to measure the radio magnetotelluric (RMT) signals from distant radio transmitters with the objective of mapping and modeling electric resistivity structures below a river or lake. The acquisition system is towed by a boat; therefore, we call the technique boat-towed RMT. The data acquisition is fast with a production rate of approximately 1 km/hr using a nominal sampling spacing of 10–15 m. Given the ample number of radio transmitters available in most parts of the world, the method can be used for near-surface studies of various targets. We have developed boat-towed RMT measurements on Lake Mälaren near the city of Stockholm in Sweden to determine the feasibility of the method. Approximately 15 km of RMT data were collected during three days above a planned 60-m-deep bypass tunnel with the goal of providing information on the bedrock depth and possible weak zones within the bedrock. The measured resistivity and phase data were of high quality with errors on the order of a few percent. The resistivity models from 2D inversion of the data showed a good correlation with available geologic data in resolving bedrock depth and also resistivity layering within the lake. Resistivity maps derived from the dense 2D models suggested a northeast–southwest-striking low-resistivity zone at less than a 30-m depth. The zone likely represents fractured crystalline bedrock. The boat-towed RMT technique is well suited for water bodies with moderate electric resistivity such as in brackish and freshwater environments.

INTRODUCTION

Using geophysical methods in solving near-surface engineering problems is rapidly increasing. There are a vast number of publications covering a wide range of hydrological (e.g., Rubin and Hubbard, 2005; Hördt et al., 2007; Slater, 2007), environmental (e.g., Bastani et al., 2012; Chen et al., 2013; Revil et al., 2013), and engineering applications including underground-construction studies (e.g., Danielsen and Dahlin, 2009; Malehmir et al., 2013, 2015). These mainly focus on land (or downhole) geophysical data acquisitions and interpretation. Okazaki et al. (2011) present an application of airborne electromagnetic (AEM) and magnetic measurements to study of a long tunnel in Japan. Results of the survey were used for detailed planning of geotechnical investigations. Christensen et al. (2015) carry out an AEM survey to supplement geotechnical investigations for a highway construction project in Norway. They develop an automated algorithm to extract the depth to bedrock using borehole and AEM data. There are a few engineering examples that demonstrate the capability of geophysical measurements, especially electric and electromagnetic (EM) methods, on lakes, rivers, or streams (e.g., Nyquist et al., 2008; Toran et al., 2010). Day-Lewis et al. (2006) present results of two case studies that demonstrate the usage of continuous resistivity profiling for identifying the spatial distribution of submarine groundwater discharge and subbottom freshwater. The measurements were performed by a boat towing an array of 12 electrodes with a dipole-dipole electrode configuration. Heaney et al. (2007) and Nyquist et al. (2009) show a case study using multiple resistivity surveys at Lake Lacawac, in northeastern Pennsylvania. They use two types of resistivity surveys, a continuous resistivity profil-

Manuscript received by the Editor 10 November 2014; revised manuscript received 4 July 2015; published online 15 October 2015.
[1]Geological Survey of Sweden, Uppsala, Sweden. E-mail: mehrdad.bastani@sgu.se; lena.persson@sgu.se.
[2]Uppsala University, Department of Earth Sciences, Uppsala, Sweden. E-mail: suman.mehta@geo.uu.se; alireza.malehmir@geo.uu.se.

ing in which a multielectrode cable was towed parallel to the shore to image spatial resistivity variations in a lake and a follow-up resistivity data acquisition using cables laid on the lake bottom perpendicular to the shoreline. The latter was carried out to study finer scale zonation from the shore influenced by seepage. Barrett et al. (2005) report results from a survey that they carry out using a transient EM (TEM) system deployed to monitor the influx of saline water through subriverbed sediments in the Murray River, South Australia. They use a floating setup of a commercial fast-sampling TEM system that was sensitive to resistivity variations at depths of less than 50 m. The survey along a 40-km section of the river imaged a range of subriverbed resistivities.

Hatch et al. (2010) present a study to define the variations in riverbed salt load using several geophysical techniques including "instream" towed TEM and towed direct current resistivity systems. Moreover, they conduct airborne-frequency-domain helicopter measurements. They compare the results from all these surveys and deduce that ground-based methods have superior resolution whereas the airborne data offer deeper penetration. Mollidor et al. (2013) develop a floating in-loop TEM method field setup, the so-called float-TEM. The system consists of a transmitter and receiver of 18×18 and 6×6 m^2, respectively. With this setup, in-loop TEM measurements can be carried out on the surface of freshwater lakes to model geometry and thickness of sediments below lakes with the aim of optimizing drill locations. The system is tested in Eifel, Germany, on Lake Holzmaar to unravel lacustrine sediments. The measurements were used as paleoclimatic proxy data.

To the best of our knowledge, we have for the first time developed a new concept using tensor radio magnetotelluric (RMT) measurements on lakes, which we call boat-towed RMT. We provide detailed information about the method including the setup, field procedures, and data processing. We also show part of the results from a field campaign in which we carried out the boat-towed RMT measurements on a lake located in an urban area close to the city of Stockholm. The RMT data collected in this study were inverted in 2D to model the electric resistivity variations down to approximately 60-m depth. The resulting models were then compared with the existing geologic and water depth data.

RMT METHOD

The RMT method uses EM signals from distant radio transmitters in the very low frequency (VLF, 15–30 kHz) and low-frequency ranges (30–300 kHz). Compared with the traditional VLF measurements, RMT covers a wider frequency range and the data carry information about the absolute resistivity values of underlying structures.

The interaction between the primary EM signal and subsurface electric resistivity structures induces secondary EM fields that can be measured and used to model electric resistivity of near-surface structures down to a maximum depth of approximately 300 m. Pedersen et al. (2006) study the distribution of RMT transmitters in Europe. They analyze the RMT data acquired in Spain, the Netherlands, Hungary, and Sweden. Their study reveals that depending on the site location in Europe, a reasonable number of radio transmitters with a horizontal magnetic field signal-to-noise ratio (S/N) of ≥ 12 dB exists in the RMT frequency range. The depth penetration of the RMT method is a function of signal frequency and the electric resistivity of the materials and varies from a few meters to a few hundred meters. Ground-based RMT data are acquired similar to MT measurements in which three components of the magnetic field (two horizontal and one vertical) and two horizontal components of the electric field are registered simultaneously. The measured time series are Fourier transformed to estimate the frequency-dependent earth EM transfer functions, namely, the impedance tensor $\mathbf{Z}$ and the tipper vector $\mathbf{T}$. In the frequency domain, $\mathbf{Z}$ and $\mathbf{T}$ are defined as

$$\begin{bmatrix} E_x(f) \\ E_y(f) \end{bmatrix} = \mathbf{Z}(f) \begin{bmatrix} H_x(f) \\ H_y(f) \end{bmatrix}, \quad \mathbf{Z}(f) = \begin{bmatrix} Z_{xx}(f) & Z_{xy}(f) \\ Z_{yx}(f) & Z_{yy}(f) \end{bmatrix} \tag{1}$$

and

$$[H_z(f)] = \mathbf{T}(f) \begin{bmatrix} H_x(f) \\ H_y(f) \end{bmatrix}, \quad \mathbf{T}(f) = [A(f) \quad B(f)], \tag{2}$$

where E and H are the electric and magnetic fields and subscripts x, y, and z represent the two horizontal and vertical measurement directions, respectively.

The impedance tensor is complex and frequency dependent. For a layered 1D earth model, the diagonal elements of the impedance tensor (Z_{xx}, Z_{yy}) are zero, $Z_{xy} = -Z_{yx}$, and the apparent electric resistivity and phase of impedance are calculated from

$$\rho_a(f) = \frac{|Z(f)|^2}{2\pi f \mu_0} \quad \text{and} \quad \phi(f) = \arg[Z(f)], \tag{3}$$

where f is the signal frequency, and μ_0 is the magnetic permeability of the vacuum. In a 2D earth model case, assuming a profile perpendicular to the strike of resistivity structure, the diagonal elements of the impedance tensor are zero and the apparent resistivity is directionally dependent, and it is defined in two perpendicular directions known as transverse electric and transverse magnetic. Determinant of the impedance tensor defined as

$$Z_{\text{det}}(f) = [Z_{xx}(f)Z_{yy}(f) - Z_{xy}(f)Z_{yx}(f)]^{1/2} \tag{4}$$

is complex and rotationally invariant and is used for modeling purposes (e.g., Pedersen and Engels, 2005; Smirnov and Pedersen, 2009; Bastani et al., 2011).

A considerable number of publications demonstrate the different applications of RMT method for near-surface geophysical investigations. The RMT method was first introduced by Müller and his group in the Centre d'Hydrogéologie, Université de Neuchâtel. They carried out scalar RMT using an RMT-R instrument with the extended frequency range of 12–240 kHz to study a porous aquifer in the Cornol area, Switzerland (Turberg et al., 1994). Since then, several workers have used the same instrument for various near-surface applications (e.g., Tezkan el al., 1996, 2000; Persson et al., 2001).

Bastani (2001) introduce a new instrument, the EnviroMT, that was developed at Uppsala University in collaboration with Metronix GmbH in Germany. The instrument performs tensor RMT measurements. Several publications throughout the years (e.g., Pedersen et al., 2006; Sohlenius et al., 2008; Bastani et al., 2009; 2013; Persson et al., 2011; Shan et al., 2013, 2014) demonstrate the capability of the tensor RMT measurements for different near-surface applications. The system was even used for 3D RMT data acquisition at a hydrocarbon-contaminated site in Italy (Bastani et al., 2012).

Boat-towed RMT setup

A schematic of the boat-towed RMT setup developed at the Geological Survey of Sweden (SGU) is shown in Figure 1. The setup is nearly the same as the one used for the land measurements; however, we used the EnviroMT system for lake measurements. The EnviroMT system comprises two main parts, namely, analog and digital. The analog components are, for example, electric field dipole (EFD) sensors, 3C magnetic field sensor (MFS) box, analog filter (AF) box including low- and high-pass filters and other electronics. The MFS and AF boxes are mounted on a floating platform mainly made up of Styrofoam and wood. The EFD sensors are assembled on wooden arms with an adjustable length that are attached to the floating platform and can easily float on the water surface (Figure 2). The platform is towed by a motorboat using a 7-m-long wooden arm to avoid disturbances from the boat's engine and data acquisition system (DAQ). The analog signal is transferred to the digital part via a 10-m-long cable. The digital part is assembled in a white plastic box, which we refer to as the DAQ box hereafter. The main electronic parts in the DAQ box are a central computer, an analog-to-digital converter and a digital signal processor. The tensor RMT data are acquired while the system is towed. The data acquisition time depends on the selected number of stacks (to increase the S/N). The measurement locations are recorded using a handheld GPS system. The accuracy of the measurement location can be improved considerably if a differential GPS (DGPS) system is used next to the AF and MFS boxes.

RMT data processing

The raw field data are the stacked auto- and crosspowers of the five measured EM components at selected transmitter frequencies. Bastani and Pedersen (2001) provide a detailed description about RMT data processing. We used the same procedure as introduced by them to process the boat-towed RMT data acquired in this study. The main RMT frequency band (10–250 kHz) is split into nine overlapping subbands of one-octave width. The RMT transfer functions and their standard deviations are estimated using a band-averaging technique explained for example by Pedersen (1982). Although these values are estimates using a certain processing technique, for simplicity and to avoid confusion with the estimated data from the inversion, we refer to them as the measured data.

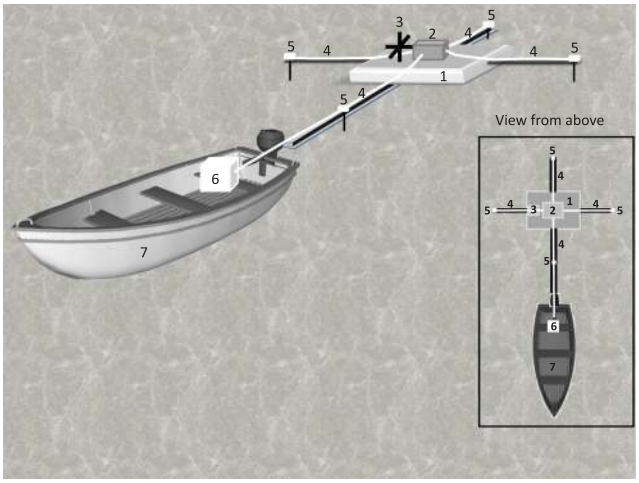

Figure 1. Sketch of the boat-towed RMT setup. (1) Floating platform, (2) central AF box (3) 3C MFS, (4) arms and cables for electric field measurements, (5) electric buffer amplifiers connected to the still electrodes floating in water, (6) central processing unit, and (7) motorboat used for towing.

Position correction

The EnviroMT system in its current form is not equipped with a built-in GPS system, and, therefore, we registered the coordinates using a handheld GPS that was located in the boat. As shown in Figures 1 and 2, the magnetic/electric sensors (central measurement point) are towed by the boat and, therefore, there is a fixed offset between the measured and the real position of the sensors. This will have an adverse effect on the interpretation of the location and subsurface resistivity features. To correct for the positioning errors, the measured coordinates in the boat had to be shifted to the sensor positions. Because the distance between the boat and the sensors is fixed, the heading angle of the boat was required to correct the positioning errors. The heading angle was estimated using the geodetic positions of consecutive measurements assuming a fixed direction between them. This is a rather robust assumption considering the low speed of the boat and extremely calm weather condition during the data acquisition. The correction will be even more accurate in the future when the setup is equipped with a DGPS device.

Platform attitude bias

Figure 2 shows a photo of the platform used in this study. Given the calm weather conditions, the platform was steady and stable when towed by the boat on the lake water. Bastani and Pedersen (1997) discuss the error on the magnetic transfer functions (tippers) introduced by variations in aircraft attitude in the airborne VLF measurements. Here, we have the same type of attitude variations when moving the measurement platform. We use the same arguments and define three attitude angles, the so-called Euler angles, as the heading (rotation around the axes perpendicular to the water surface, or the z-axes), pitch (rotation around the axes perpendicular to the lines, or the y-axes), and roll (rotation around the axes along the line, or the x-axes). In our study, no devices were used to measure these angles. A simple case describing the effect of changes in

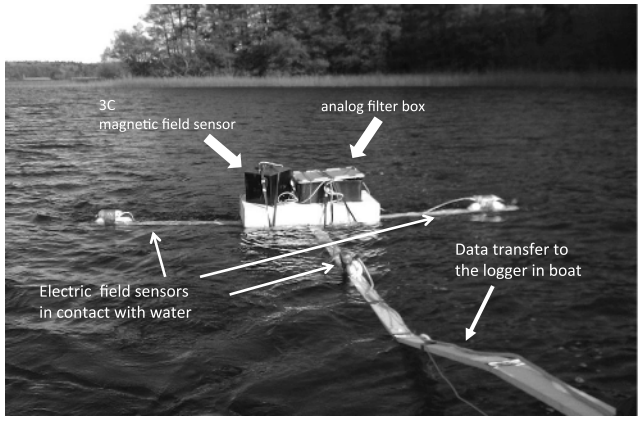

Figure 2. A photo showing the boat-towed RMT setup while measuring on the Lake Mälaren close to Stockholm, Sweden. Different components of the setup are also shown (see also Figure 1).

the roll angle is provided here, and for more complicated cases, the readers are referred to Bastani and Pedersen (1997).

Assume that a water wavefront traveling in the y-direction meets the platform and results in a rotation of the platform around the x-direction with an angle of α. This introduces a bias on the electric and magnetic field components measured in y- and z-directions. If we assume a 1D earth model, then the apparent electric resistivity in the rotated platform coordinate system $(x'y'z')$ can be calculated using

$$\rho_a' = C\left|\frac{E_{x'}}{H_{y'}}\right|^2, \tag{5}$$

Figure 3. (a) The Bypass Stockholm project plan. The green line is the planned track, and the frame on the top-right corner shows the location of the study area in Sweden. (b) Cross section of part of the planned tunnels (marked with the dashed white box in panel [a]) below Lake Mälaren. Sites 1, 2, and 3 are where the case study was conducted.

where C is a constant. The true apparent resistivity in a fixed coordinate system (xyz) is given by

$$\rho_a = C\left|\frac{E_x}{H_y}\right|^2. \tag{6}$$

We estimate the bias (in percentage) introduced on the calculated apparent resistivity due to the attitude variation using

$$\frac{\Delta\rho}{\rho}\% = \tan^2\alpha \times 100. \tag{7}$$

For example, the bias for a fixed rotation angle of 10° is approximately 3.1%. Considering the oscillating nature of the rotation angle and the recording time of 15 s, the mean/effective rotation angle is smaller than 10°, which results in a very small bias. This bias is on the order of the measurement errors. It can easily be shown that the attitude of the platform does not affect the phase of the impedance tensor. Consequently, with the weather conditions we had during the measurements, the attitude bias on the acquired data set can be assumed to be negligible.

FIELD EXAMPLE FROM BYPASS STOCKHOLM PROJECT

Based on the latest information, the population of the metropolitan area of Stockholm, the capital city of Sweden, has reached more than 2 million. This includes more than one-fifth of the country's entire population. With the increasing population, the traffic infrastructure has been overloaded and has caused various problems, for example, air pollution and lost time in traffic. To ease the traffic and reduce its environmental impacts, the Swedish Transport Administration (Trafikverket) has planned various underground infrastruc-

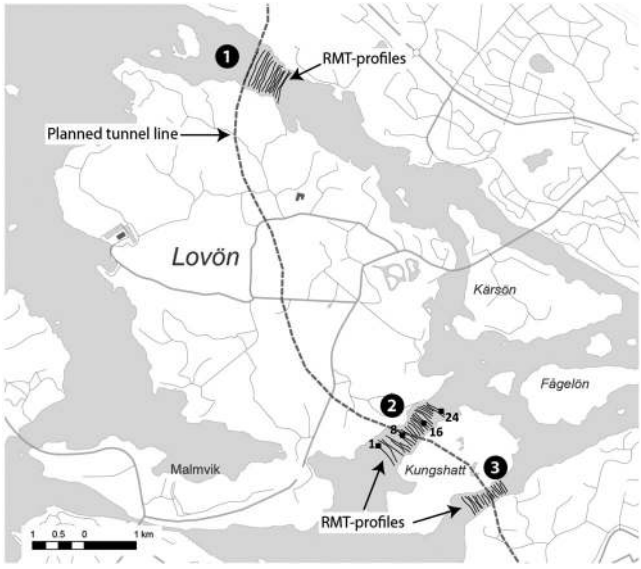

Figure 4. Detailed location map of the boat-towed RMT profiles (see the areas marked by 1, 2, and 3) in the study area over three WPs. The dashed line indicates the route of the planned tunnel with a maximum depth of approximately 60 m below the surface (see Figure 3b). The black squares on lines 1, 8, 16, and 24 indicate locations of the stations selected for presentation of data quality shown in Figure 5.

ture projects, one being the so-called Bypass Stockholm (Förbifart Stockholm). The project is planned for 10 years and aims for a new underground (primarily) motorway with a total length of nearly 21 km connecting the southern and northern parts of the city (see Trafikverket, 2015). This will also facilitate traffic on the European highway E4 that runs from the south of Sweden to its northern parts. The bypass is located west of Stockholm and has been under investigation for several years (Figure 3). To our knowledge, the link will be one of the longest road tunnels in the world. Trafikverket estimates that 140,000 vehicles per day will pass through the Stockholm bypass by 2035.

The approved design has taken into account the impact on sensitive natural and cultural environments, and 18 km of the motorway link will be via rock tunnels. According to Trafikverket, the construction of the access tunnels (ramps) and three temporary harbors will start by summer 2015. The tunnel passes below Lake Mälaren at three localities marked 1 to 3 in Figure 3. The lake holds freshwater and is separated from the Baltic Sea by the Stockholm Sluice. Bypass Stockholm is likely one of the first large underground infrastructure tunnels that is going to be developed on the mainland Sweden. Approximately 7% of Swedish land is covered by water, and one would expect more of these types of projects to be initiated. This highly motivates the development of marine geophysical equipment for carrying out shallow water investigations.

Data acquisition and quality

Prior to the main data acquisition, we performed several tests close to and at the study area to check the feasibility of the concept and the quality of the RMT signals. The tests showed that the EM signals from a total number of 20 to 27 transmitters with S/N >10 dB could be used for the RMT measurements on Lake Mälaren at the three selected sites (Figure 4). The sites are hereafter referred to as water passages (WPs). The WPs isolate three islands, namely, Lovön, Kungshatt, and Sätra (Figure 4). The measurements took one day per site with 5 hr of data acquisition per day. The floating platform was towed by a motorboat (Figures 1 and 2) with an average speed of approximately 0.5 m/s. The number of stacks was 50 corresponding to a data acquisition time of approximately 15 s per measurement point and 15–17-m station spacing. We covered a total length of approximately 15 km (54 lines) during the three days of data acquisition (Figure 4).

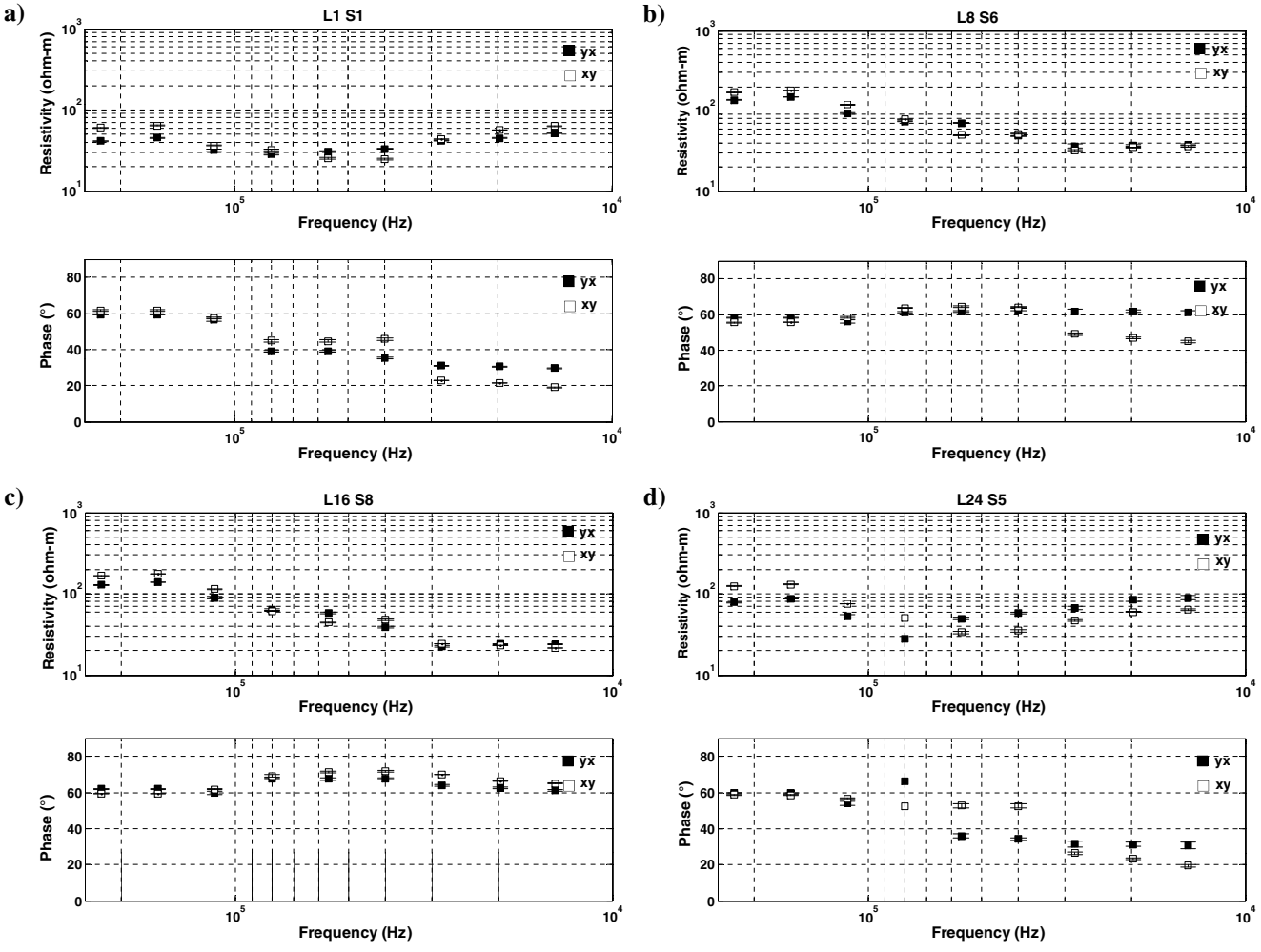

Figure 5. Boat-towed RMT field data for a selection of stations along the lines at site 2 (see Figure 4 for locations). The white and black squares are the *xy* and *yx* data, respectively. (a) Line 1 and station 1, (b) line 8 and station 6, (c) line 16 and station 8, and (d) line 24 and station 5. Note that at each station, the frames at the top are resistivities and those at the bottom are phases.

Traditionally, the measured apparent resistivities and phases from off-diagonal impedance elements (*xy* and *yx* in equation 1) are presented at all stations. Considering the huge volume of the collected boat-towed RMT data in this study, we just present the measured data in the *xy*- and *yx*-directions at four stations from lines 1, 8, 16, and 24 at site 2 (for locations, see Figure 4). Figure 5 shows the measured apparent resistivities and phases at the four selected stations at site 1. For each station, the data are presented in two frames with resistivities at the top and the phases at the bottom. Note that *x* and *y* denote directions along and perpendicular to the lines, respectively.

Generally, the data quality is good with small estimated errors that are on the order of 2%–3%. The errors are large at some stations for certain frequencies (see, for example, 60–120 kHz in Figure 4d). This behavior can to a large extent depend on the number of available radio transmitters, which has also been reported by Bastani and Pedersen (2001) and Bastani et al. (2011). We have also observed large error bars at some profiles that might be due to EM noise generated from power cables laid on the bottom of the lake.

It is important that these cultural noises associated with the city infrastructure are identified and processed before the data can be further used as input for inversion and modeling. We used parametric representation combined with the truncated singular value decomposition (TSVD) regularization of Bastani and Pederson (2001) to estimate reliable impedance tensors. The TSVD method takes into account the various complexities associated with the RMT signal, for example, the uneven distribution of radio transmitters and the deviation in their azimuths within a given band of one-octave width. Moreover, it uses a robust technique to reject signal from nearby noise sources by estimating prediction errors at each transmitter frequency (for details, see Bastani and Pedersen, 2001).

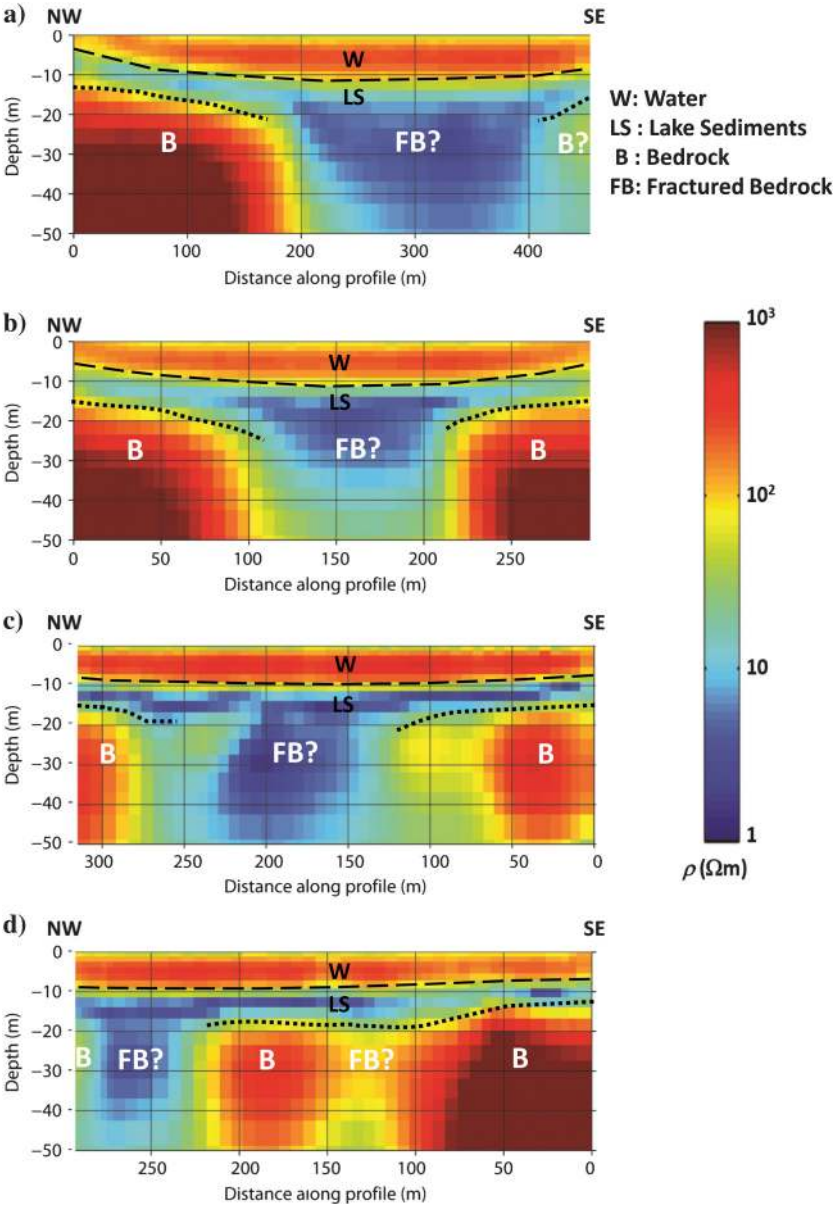

Figure 6. Selected 2D resistivity models along four lines located on the WP between Lovön and Kungshatt: (a) line 1, (b) line 9, (c) line 16, and (d) line 24. The resistive bedrock is marked by B, possible low-resistivity-fractured bedrock by FB, water by W, and lake sediments by LS.

RESULTS AND DISCUSSION

We carried out independent 2D inversions of the tensor RMT data along all the lines. For this, we used the modified version of the finite-difference inverse code REBOCC (Siripunvaraporn and Egbert, 2000; Kalscheuer et al., 2008). The determinant RMT data were used in the 2D inversions. The determinant data are rotationally invariant, and it is preferable to use them when the regional strike is unknown (Pedersen and Engels, 2005), or as in our case, when it is difficult to keep the electric dipoles and magnetic antennas in a preferred direction while measuring on a moving boat. Optimal finite-difference mesh specification is important to obtain accurate modeling results. In this case, the shallowest blocks were 1 m thick and the deepest ones were approximately 1200 m. The distance between measurement points varied along the lines, and we used a variable block width with two blocks/measurements. The regularization used was of the Occam type (Kalscheuer et al., 2008). We used an error floor of 4% for the apparent resistivity and phase, respectively, to avoid data overweighting. Along most of the lines, a normalized overall root mean square of three was achieved. The 2D resistivity models of four selected lines that are evenly located on the WP between Lovön and Kungshatt (for the locations of the lines, see Figure 4) are shown in Figure 6.

A reasonable correlation is observed between the resistivity models from the 2D inversions of determinant data along these lines. Four distinct resistivity features can be observed in almost all of the resistivity models. The features are marked in the models using different labels (Figure 6).

The estimated resistivities of each structure, e.g., the water body (marked by W), are consistent across the lines, demonstrating stability and accuracy of the data acquisition system (DAS) and data processing techniques used. The key geologic targets in this study have been the bedrock depth/surface (marked by B) and possible fractures/fracture zones within the bedrock (marked by FB). As shown in Figure 6, the lake water has a resistivity of up to 300 ohm-m with a well-defined bottom (marked by dashed lines) that is shallower at both ends of the models closer to the shorelines. The lake sediments (marked by LS), on the other hand, have low resistivity (less than 10 ohm-m) with varying thickness along the lines. The lake sediments are generally thicker in the middle of the lines. The crystalline bedrock is the most resistive feature (>500 ohm-m) and is mainly resolved at both ends of the resistivity models. (The approximate bedrock surface is marked by dotted lines in Figure 6.) The bedrock is interpreted at an approximately 20-m depth where the lake sediments are thinnest. The bedrock is not resolved at locations where the low-resistivity lake sediments are thicker than 10 m. The lake sediments screen the radio signals implying a depth penetration limitation (Spies, 1989; Hung, 2005). The low-resistivity feature in the models shows an abrupt increase in their thickness mainly in the middle of the lines, which implies either a change in the thickness of the lake sediments or a reduction in bedrock resistivity because of potential fractures filled by lakewater or fine-grained sediments (e.g., clays). At some locations (e.g., 100–150-m distance in Figure 6d), the thickness of the lake sediments is less than 10 m and the underlying resistive feature (bedrock) contains low-resistivity zones within it. This likely indi-

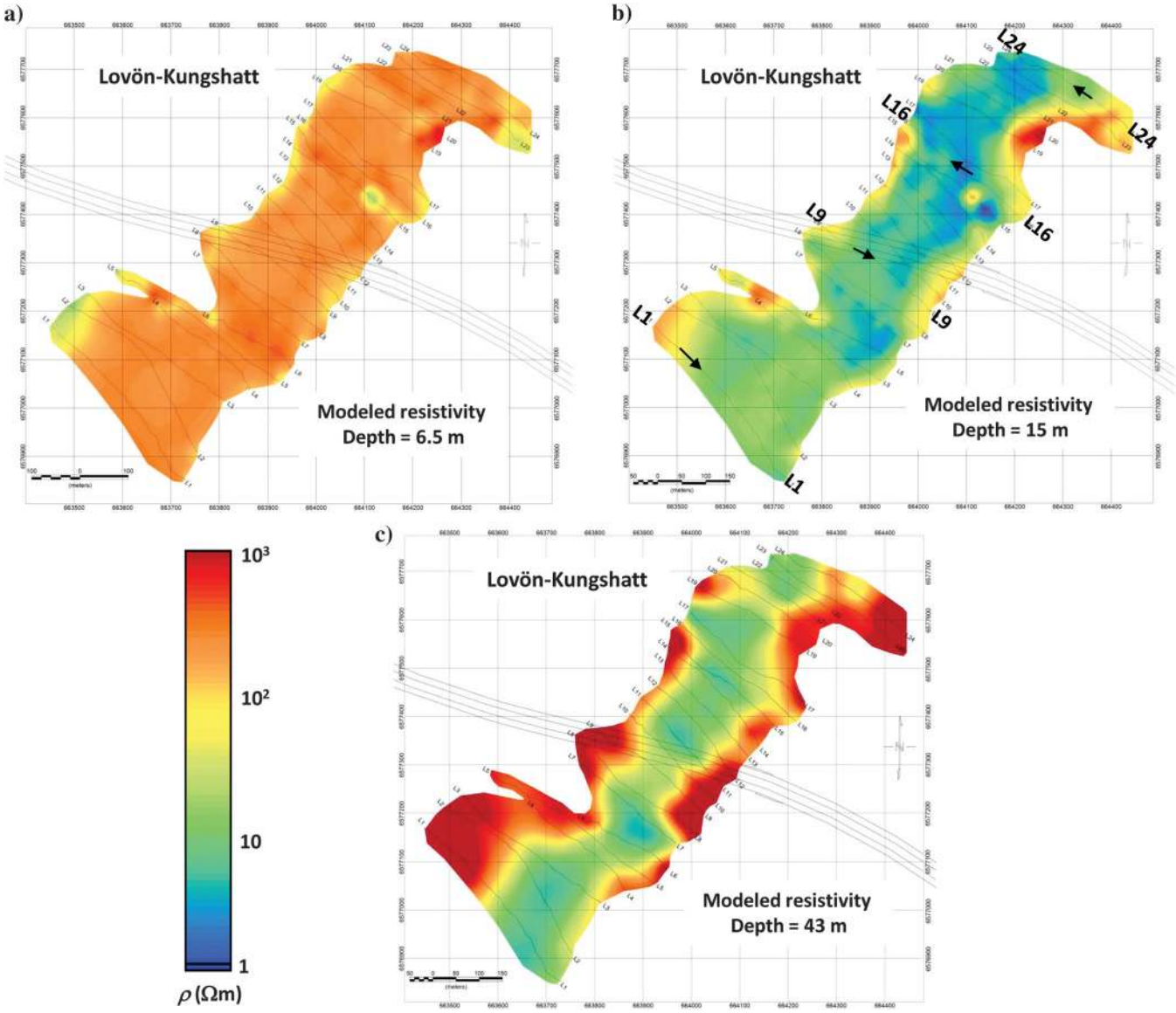

Figure 7. Resistivity slices from 2D inversion models along the lines located on the WP between Lovön and Kungshatt. Resistivity slices at (a) 6.5, (b) 15, and (c) 43 m. The RMT lines are shown with lines labeled by their numbers. The models shown in Figure 6 are marked by larger labels, and black arrows indicate the direction of the measurements. Four parallel and long black lines passing across the depth slices represent the path of the planned tunnel in area 2.

cates potential fractures or weak zones in the bedrock. One should also consider that because of the smoothing nature of the Occam inversion, depth to the bottom (thickness) of the lake sediments are ambiguous, especially where they are thicker than 10 m. It is also a well-known phenomenon that the EM methods are poor at resolving depth to high-resistivity structures.

Once the 2D resistivity models along all the lines were obtained, they were gridded together at different depths to allow resistivity depth slices. Figure 7 shows three depth slices from the modeled resistivities. The depths are selected with regard to the key features observed in the resistivity models. Figure 7a shows variations in the modeled resistivity at a 6.5-m depth that is mainly within the water body. The resistivity at this depth has values of approximately 210 ± 80 ohm-m with the highest variations mainly observed closer to the shorelines where the water depth is less than 6.5 m. To verify the reliability of the resistivity models, we obtained water depth information from the SGU marine geologic database. Figure 8a shows a water-depth map of the study area. The water depth reaches its maximum value of 13 m at the southwestern part of the study area (beneath L1 to L4). A comparison with the resistivity models shown in Figure 6 suggests that the estimated water depths correlate well with this water-depth information. The white line in Figure 8a illustrates the boundary of the postglacial clays mapped by marine geologic studies. An interesting correlation can be observed between the resistivity slice at the 15-m depth (Figure 7b) and a map of the sediments below the water body (Figure 8b). A low-resistivity zone at this depth follows the boundaries of the mapped postglacial clays. Interestingly, the resistivity increases in the southwestern part of the study area (Figure 7b) in which the sediments containing gas are reported in SGU's marine database.

The thickness of the clays in the area generally varies between a few centimeters to approximately 5 m. At some locations, there are moraine sediments below the clays that result in an increase in the thickness of the sediments. This implies that the overall thickness of the materials over the crystalline bedrock (lake water and lake sediments) is less than 30 m, which in turn implies that the resistivity models below this depth should depict the variations in the electric resistivity of the bedrock. Looking at Figure 7c, one observes that there is a southwest–northeast-striking low-resistivity zone at a depth of 43 m that has a varying width of approximately 50–100 m. The width is probably biased (overestimated) because of the Occam regularization used in the inversion. It dictates smoothing in the lateral and vertical directions, which generates anomalous zones that are wider and thicker than their true dimensions.

The bedrock map of the area provided by SGU (Persson, 2001) suggests that the planned tunnel will mainly be excavated within granitic and metasedimentary rocks. Geologic observations on the outcrops indicate that there are fractured zones in the crystalline bedrock with widths that vary between 1 and 5 m. The fractures are partly filled with clay, graphite, and chlorite, which reduce the bulk resistivity of the bedrock considerably. We used an average horizontal cell size of 8 m in the inversion (half the station spacing), which is the smallest width to be resolved in the resistivity models. This implies that true fractures within the bedrock (e.g., 1 m wide) with low resistivities might be somewhat imaged as nearly vertical wider zones with higher resistivities in the models. However, if the depth penetration is large enough, these zones must be considered as good indicators of fractures at depth.

The acquired boat-towed RMT data provide good grounds for a detailed 3D modeling and inversion, which will be considered in a separate study. Detailed 2D and 3D synthetic modeling to analyze the lateral and vertical resolution of the lake RMT data should also be considered. We also have access to the velocity models from processing of marine refraction seismic data acquired in the same area and also the data from a horizontal borehole in site 2. All these data will be used to constrain modeling and interpretation of the RMT data.

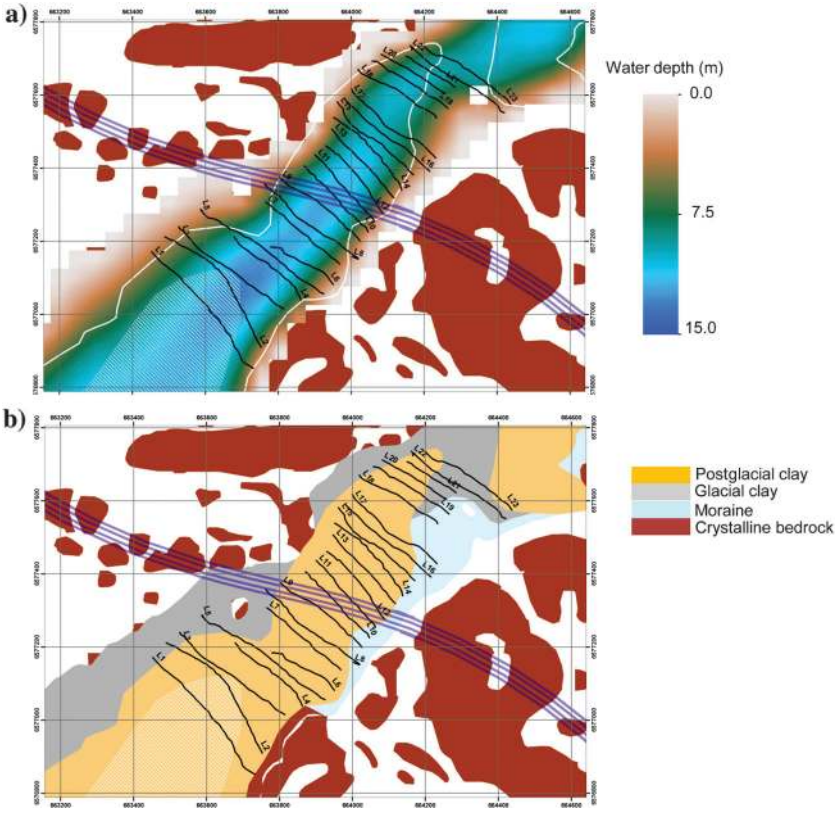

Figure 8. (a) Measured water depth within the frame of marine geologic mapping conducted by SGU. The outcrops of high-resistivity crystalline bedrock are shown in dark red. The white lines indicate the boundaries of the low-resistivity postglacial clays. (b) Map of sediments from SGU's database. The black lines show the RMT lines, and the thicker violet lines show the planned tunnels of the Stockholm bypass project. The hashed area with white line marks the marine sediments that apparently contain biogenic gas.

CONCLUSIONS

A new boat-towed RMT technique has been developed, used, and proven to be practical for various near-surface applications. The floating setup is stable on still water to moderately wavy water, implying that the bias imposed on the data by variations in the platform attitude is negli-

gible. The acquired data have reasonably good to high quality within an acceptable error level of up to 2%–3%. The data acquisition is significantly fast with a production rate of 1 km/hr with an average station spacing of 15 m. The three-day measurements on Lake Mälaren in the city of Stockholm resulted in totally 15-km-long 2D resistivity models from the inversion of determinant resistivity and phase data. The resistivity models show good correlation with the available marine geologic measurements and existing geologic field observations in the study area. The modeled water depths are well-estimated and the depth to the crystalline bedrock wherever the thickness of the lake sediments are less than 10 m is well-resolved and hence reliable. A southwest–northeast-striking low-resistivity zone is found in the bedrock that is likely a potential fracture zone filled with less-resistive materials such as clay minerals and graphite. The width and depth of the zone are uncertain in part due to the regularization used in the inversion and the limited signal frequency that strongly limits the penetration depth.

The Lake Mälaren case study illustrates the capability of the boat-towed RMT system, and we expect that the system could be used in the near future for other applications on moderately resistive water bodies. The technique can be further improved by implementing a DGPS receiver to the DAS for an accurate geodetic positioning. With the same system, it is possible to acquire controlled-source audiomagnetotellurics data at frequencies down to 1000 Hz, which should increase the penetration depth at least three times more. However, this requires some modification to the DAS and will slow down the production rate — an issue that will be investigated in future studies.

ACKNOWLEDGMENTS

The authors would like to thank the SGU for financing the construction of the floating system via internal research project 35219. S. Mehta's Ph.D. work and A. Malehmir's contributions are sponsored by Formas, Befo, SBUF, and Skanska through Trust 2.2 project (www.trust-geoinfra.se). Three reviewers and the associate editor provided critical and useful comments that improved an early version of this paper and for which we are grateful.

REFERENCES

Barrett, B., G. Heinson, M. Hatch, and A. Telfer, 2005, River sediment salt-load detection using a water-borne transient electromagnetic system: Journal of Applied Geophysics, **58**, 29–44, doi: 10.1016/j.jappgeo.2005.03.002.

Bastani, M., 2001, EnviroMT - A new controlled source/radio magnetotelluric system: Ph.D. thesis, Uppsala University.

Bastani, M., J. Hübert, T. Kalscheuer, L. B. Pedersen, A. Godio, and J. Bernard, 2012, 2D joint inversion of RMT and ERT data versus individual 3D inversion of full tensor RMT data: An example from Trecate site in Italy: Geophysics, **77**, no. 4, WB233–WB243, doi: 10.1190/geo2011-0525.1.

Bastani, M., A. Malehmir, N. Ismail, L. B. Pedersen, and F. Hedjazi, 2009, Delineating hydrothermal stockwork copper deposits using controlled-source and radio-magnetotelluric methods: A case study from northeast Iran: Geophysics, **74**, no. 5, B167–B181, doi: 10.1190/1.3174394.

Bastani, M., and L. B. Pedersen, 1997, The reliability of aeroplane attitude determination using the main geomagnetic field with application to tensor VLF data analysis: Geophysical Prospecting, **45**, 831–841, doi: 10.1046/j.1365-2478.1997.480294.x.

Bastani, M., and L. B. Pedersen, 2001, Estimation of magnetotelluric transfer functions from radio transmitters: Geophysics, **66**, 1038–1051, doi: 10.1190/1.1487051.

Bastani, M., L. Persson, M. Beiki, and R. Harinen, 2013, A radio magnetotelluric study to evaluate the extents of a limestone quarry in Estonia: Geophysical Prospecting, **61**, 678–687, doi: 10.1111/j.1365-2478.2012.01101.x.

Bastani, M., A. Savvaidis, L. B. Pedersen, and T. Kalscheuer, 2011, CSRMT measurements in the frequency range of 1–250 kHz to map a normal fault in the Volvi basin, Greece: Journal of Applied Geophysics, **75**, 180–195, doi: 10.1016/j.jappgeo.2011.07.001.

Chen, J., S. Hubbard, and K. Williams, 2013, Data-driven approach to identify field-scale biogeochemical transitions using geochemical and geophysical data and hidden Markov models: Development and application at a uranium-contaminated aquifer: Water Resources Research, **49**, 6412–6424, doi: 10.1002/wrcr.20524.

Christensen, C. W., A. A. Pfaffhuber, H. Anschütz, and T. F. Smaavik, 2015, Combining airborne electromagnetic and geotechnical data for automated depth to bedrock tracking: Journal of Applied Geophysics, **119**, 178–191, doi: 10.1016/j.jappgeo.2015.05.008.

Danielsen, B. E., and T. Dahlin, 2009, Comparison of geoelectrical imaging and tunnel documentation at the Hallandsås Tunnel, Sweden: Engineering Geology, **107**, 118–129, doi: 10.1016/j.enggeo.2009.05.005.

Day-Lewis, F. D., E. A. White, C. D. Johnson, J. W. Lane, and J. Belaval, 2006, Continuous resistivity profiling to delineate submarine groundwater discharge — Examples and limitations: The Leading Edge, **25**, 724–728, doi: 10.1190/1.2210056.

Hatch, M. A., T. Munday, and G. S. Heinson, 2010, A comparative study of in-river geophysical techniques to define variations in riverbed salt load and aid managing river salinization: Geophysics, **75**, no. 4, WA135–WA147, doi: 10.1190/1.3475706.

Heaney, M. J., J. E. Nyquist, and L. E. Toran, 2007, Marine resistivity as a tool for characterizing zones of seepage at Lake Lacawac, PA: Proceedings of the 20th EEGS Symposium on the Application of Geophysics to Engineering and Environmental Problems, 1139–1149.

Hördt, A., R. Blaschek, A. Kemna, and N. Zisser, 2007, Hydraulic conductivity estimation from induced polarisation data at the field scale — The Krauthausen case history: Journal of Applied Geophysics, **62**, 33–46, doi: 10.1016/j.jappgeo.2006.08.001.

Huang, H., 2005, Depth of investigation for small broadband electromagnetic sensors: Geophysics, **70**, no. 6, G135–G142, doi: 10.1190/1.2122412.

Kalscheuer, T., L. B. Pedersen, and W. Siripunvaraporn, 2008, Radiomagnetotelluric two-dimensional forward and inverse modelling accounting for displacement currents: Geophysical Journal International, **175**, 486–514, doi: 10.1111/j.1365-246X.2008.03902.x.

Malehmir, A., M. Bastani, C. Krawzyck, M. Gurk, N. Ismail, U. Polom, and L. Persson, 2013, Geophysical assessment and geotechnical investigation of quick-clay landslides — A Swedish case study: Near Surface Geophysics, **11**, 341–350, doi: 10.3997/1873-0604.2013010.

Malehmir, A., F. Zhang, E. Lundberg, M. Dehgahnnejad, O. Friberg, B. Brodic, C. Döse, J. Place, M. Svensson, and H. Möller, 2015, Planning of urban underground infrastructure projects using a broadband seismic landstreamer — Tomography results and uncertainty quantifications from a case study in southwestern Sweden: Geophysics, **80**, this issue, doi: 10.1190/geo2015-0052.1.

Mollidor, L., B. Tezkan, R. Bergers, and J. Löhken, 2013, Float-transient electromagnetic method: In-loop transient electromagnetic measurements on Lake Holzmaar, Germany: Geophysical Prospecting, **61**, 1056–1064, doi: 10.1111/1365-2478.12025.

Nyquist, J. E., P. A. Freyer, and L. Toran, 2008, Stream bottom resistivity tomography to map ground-water discharge: Ground Water, **46**, 561–569, doi: 10.1111/j.1745-6584.2008.00432.x.

Nyquist, J., M. J. Heaney, and L. Toran, 2009, Characterizing lakebed seepage and geologic heterogeneity using resistivity imaging and temperature measurements: Near Surface Geophysics, **7**, 487–498, doi: 10.3997/1873-0604.2009022.

Okazaki, K., T. Mogi, M. Utsugi, Y. Ito, H. Kunishima, T. Yamazaki, Y. Takahashi, T. Hashimoto, Y. Ymamaya, H. Ito, H. Kaieda, K. Tsukuda, Y. Yuuki, and A. Jomori, 2011, Airborne electromagnetic and magnetic surveys for long tunnel construction design: Physics and Chemistry of the Earth, **36**, 1237–1246, doi: 10.1016/j.pce.2011.05.008.

Pedersen, L. B., 1982, The magnetotelluric impedance tensor — Its random and bias errors: Geophysical Prospecting, **30**, 188–210, doi: 10.1111/j.1365-2478.1982.tb01298.x.

Pedersen, L. B., M. Bastani, and L. Dynesius, 2006, Some characteristics of the electromagnetic field from radio transmitters in Europe: Geophysics, **71**, no. 6, G279–G284, doi: 10.1190/1.2349222.

Pedersen, L. B., and M. Engels, 2005, Routine 2D inversion of magnetotelluric data using the determinant of the impedance tensor: Geophysics, **70**, no. 2, G33–G41, doi: 10.1190/1.1897032.

Persson, L., 2001, Plane wave electromagnetic measurements for imaging fracture zones: Ph.D. thesis, Uppsala University.

Persson, L., I. Antal, L. B. Pedersen, and D. Claeson, 2011, Combined magnetic, electromagnetic and resistivity study over a highly conductive formation in Orrivaara, Northern Sweden: Geophysical Prospecting, **59**, 1155–1163, doi: 10.1111/j.1365-2478.2011.00998.x.

Persson, L., M. Sträng, and I. Antal, 2001, Bergrundskartan 10I Stockholm. Sveriges geologiska undersökning (report in Swedish), Ba 60.
Revil, A., M. Skold, M. Karaoulis, M. Schmutz, S. S. Hubbard, T.L. Mehlhorn, and D. B. Watson, 2013, Hydrogeophysical investigations of the former S-3 ponds contaminant plumes, Oak Ridge Integrated Field Research Challenge Site, Tennessee: Geophysics, **78**, no. 4, EN29–EN41, doi: 10.1190/geo2012-0177.1.
Rubin, Y., and S. S. Hubbard, 2005, Introduction to hydrogeophysics, *in* Y. Rubin, and S. S. Hubbard, eds., Hydrogeophysics: Springer, 3–21.
Shan, C., M. Bastani, A. Malehmir, M. Engdahl, and E. Lundberg, 2013, 3D resistivity models from inversion of controlled source- and radio-magnetotelluric (CSRMT) data at a quick-clay site in southwestern Sweden: 83rd Annual International Meeting, SEG, Expanded Abstracts, 1950–1954, doi: 10.1190/segam2013-1164.
Shan, C., M. Bastani, A. Malehmir, L. Persson, and M. Engdahl, 2014, Integrated 2D modelling and interpretation of geophysical and geotechnical data to delineate quick clays at a landslide site in southwest Sweden: Geophysics, **79**, no. 4, EN61–EN75, doi: 10.1190/geo2013-0201.1.
Siripunvaraporn, W., and G. Egbert, 2000, An efficient data-subspace inversion method for two-dimensional magnetotelluric data: Geophysics, **65**, 791–803, doi: 10.1190/1.1444778.
Slater, L., 2007, Near surface electrical characterization of hydraulic conductivity: From petrophysical properties to aquifer geometries — A review: Surveys in Geophysics, **28**, 169–197, doi: 10.1007/s10712-007-9022-y.
Smirnov, M. Yu., and L. B. Pedersen, 2009,. Magnetotelluric measurements across Sorgenfrei-Tornquist-zone in southern Sweden and Denmark: Geophysical Journal International, **176**, 443–456, doi: 10.1111/j.1365-246X.2008.03987.x.
Sohlenius, G., M. Bastani, L. Persson, and K. Lax, 2008, On the recognition of areas with problematic sulphidic sediments using multi-disciplinary data: Environmental Geology, **56**, 973–984, doi: 10.1007/s00254-008-1199-y.
Spies, B. R., 1989, Depth of exploration in electromagnetic sounding methods: Geophysics, **54**, 872–888, doi: 10.1190/1.1442716.
Tezkan, B., M. Goldman, S. Greinwald, I. Mueller, F. M. Neubauer, G. Zacher, and A. Hoerdt, 1996, A joint application of radio magnetotellurics and transient electromagnetics to the investigation of a waste deposit in Cologne, Germany: Journal of Applied Geophysics, **34**, 199–212, doi: 10.1016/0926-9851(95)00016-X.
Tezkan, B., A. Hordt, and M. Gobashy, 2000, Two-dimensional radiomagnetotelluric investigation of industrial and domestic waste sites in Germany: Journal of Applied Geophysics, **44**, 237–256, doi: 10.1016/S0926-9851(99)00014-2.
Toran, L., M. Johnson, J. Nyquist, and D. Rosenberry, 2010, Delineating a road salt plume in lakebed sediments using electrical resistivity, piezometers, and seepage meters at Mirror Lake, New Hampshire, U.S.A.: Geophysics, **75**, no. 4, WA75–WA83, doi: 10.1190/1.3467505.
Trafikverket (The Swedish Transport Administration), 2015, http://www.trafikverket.se/, accessed 15 September 2015.
Turberg, P., I. Muller, and F. Flury, 1994, Hydrogeological investigation of porous environments by audiomagnetotelluric resistivity: Journal of Applied Geophysics, **31**, 133–143, doi: 10.1016/0926-9851(94)90052-3.